A monolithic 180 nm CMOS dosimeter for wireless in Vivo Dosimetry

Radiation Measurements 84 (2016) 55–64

Contents lists available at ScienceDirect

Radiation Measurements

journal homepage: www.elsevier.com/locate/radmeas

A monolithic 180 nm CMOS dosimeter for wireless In Vivo Dosimetry

E.G. Villani [a, *], M. Crepaldi [f], D. DeMarchi [f], A. Gabrielli [b], A. Khan [c], E. Pikhay [d], Y. Roizin [d], A. Rosenfeld [e], Z. Zhang [a]

[a] STFC Rutherford Appleton Laboratory, Particle Physics Dept., UK
[b] Physics and Astronomy Dept. University of Bologna and INFN, Italy
[c] Dept. of Electronic and Computer Engineering, Brunel University, UK
[d] TowerJazz Semiconductor Ltd, Migdal Haemek, Israel and Technion, Haifa, Israel
[e] CMRP, University of Wollongong, Australia
[f] IIT, Istituto Italiano di Tecnologia, Politecnico di Torino, Italy

HIGHLIGHTS

- A Monolithic Dosimeter for real time dosimetry during radiotherapy is proposed.
- The proposed device is 1 mm3 in size and could potentially be body implantable.
- The device includes a radiation sensor and RF readout, operating in the MICS band.
- Detailed tests have been performed under radiation beam in a clinical environment.
- Reported sensitivity is 1 cGy over 50 Gy, with an accuracy of better than 3%.

ARTICLE INFO

Article history:
Received 10 July 2015
Received in revised form
25 October 2015
Accepted 18 November 2015
Available online 2 December 2015

Keywords:
In vivo dosimetry
Floating gate
MICS
Wireless

ABSTRACT

The design, fabrication and testing of a novel monolithic system-on-chip dosimeter fabricated in a standard 180 nm CMOS technology is described. The device, implementing a radiation sensor and an RF transmitter, is proposed to address the need for real-time In Vivo Dosimetry (IVD) of radiation during Linac radiotherapy sessions. Owing to its small size, of approximately 1 mm^3, such solution could be made in-body implantable and, as such, provide a much-enhanced high-resolution, real-time dose measurement to improve Quality Assurance (QA) in radiation therapy. The device transmits the related information on dose of radiation wirelessly to a remote receiver operating in the Medical Implant Communication Service (MICS) band. Comprehensive description of the various phases of this project, including the development of the radiation sensors and integrated RF transmitter to perform the readout, along with the final test results using a radiation beam, will be given.

1. Introduction: the in vivo dosimetry

The aim of this project was to design a monolithic system-on-chip, of approximate size 1 mm^3, capable of performing the real-time measurement of dose of therapeutic radiation delivered to it and to transmit the related information wirelessly to a remote receiver.

Its small size would render such proposed system potentially body implantable, a solution that could allow real-time In Vivo Dosimetry (IVD) during radiotherapy sessions of unprecedented accuracy, being performed directly or very near the treatment volume location.

The importance of IVD as QA tool has long been recognized in the medical community (Rosenfeld et al., 2006; Towards-safer-radiotherapy; Scarantino et al., 2006); recommendations reports for practical dosimetry (International Atomic Energy Agency, 2000; Izewska et al., 2002; International Atomic Energy Agency, 2007) and surveys on its usage in radiotherapy centers are also available (Nelms and Simon, 2007).

Monolithic wearable systems for wireless real-time measurement of dose of radiation have been proposed ((Shamim et al., 2008)). However, the only recent example of an implantable device, which was fabricated in a hybrid technology and which was

* Corresponding author. STFC Rutherford Appleton Laboratory, Harwell, Didcot, Oxfordshire OX11 0QX, UK.
E-mail address: Giulio.villani@stfc.ac.uk (E.G. Villani).

http://dx.doi.org/10.1016/j.radmeas.2015.11.004
1350-4487/

used in clinical practice for this purpose, is reported in Scarantino et al, (2004). Test results obtained from real patients using such device (Scarantino et al., 2008, 2005) justified the development of the project here described.

A general description of the operating principle and features of the monolithic dosimeter are shown in this paper in Section 2. Subsequent sub-sections describe the various design aspects of the dosimeter blocks, including technical details of the radiation sensors and the read out section. Section 3 describes test results of the individual elements of the dosimeter. Section 4 describes the details of the final, monolithic version of the dosimeter, including the processing phases of dicing to the required size of 1 mm^3 and bump bonding on a PCB carrier for the final radiation test. In Section 5 the description of the wireless radiation test performed with Linac in a radiotherapy center along with the obtained results are shown. Finally, in Section 6, a summary of the project and conclusions are given, along with proposed ideas on how to further develop the dosimeter towards a practical implementation usable in clinical practice.

2. Monolithic CMOS system for wireless dosimetry

The block diagram of the proposed monolithic dosimeter investigated in this project is shown in Fig. 1. This System-On-Chip (SOC) device consists of three sections, all integrated on the same silicon substrate: the radiation sensor, an analog to digital converter and an RF transmitter, the output of which drives a loop antenna.

The whole device is fabricated using a standard 180 nm CMOS technology, provided by Tower Jazz Semiconductor foundry. The target size of the final SOC was chosen to be approximately 1 mm^3, a compromise between low invasivity for a potentially body-implantable device and easiness of localization using standard clinical imaging techniques (Mahadevappa, 2009).

This project covered the design, fabrication and testing aspects of the SOC only. The other elements, that would indeed be needed for an actual implementation of IVD, including an autonomous powering, a biocompatible packaging and a custom RF receiver, were not investigated.

During the final radiation tests, the powering of the device was provided by an external small battery cell and the wireless retrieval of the data from the dosimeter was implemented using an external RF receiver and a spectrum analyzer, as described in details in Section 5.

A total of three ASIC designs were submitted to the foundry for fabrication. The first two addressed the radiation sensors and the readout section respectively. Following electrical and radiation characterization, the best performing flavors of each of these blocks were selected and in turn implemented in the third and final design. ASICs from the latest design were diced to the required size of 1×1 mm^3, initially wire bonded on a PCB carrier for initial tests and finally bump-bonded on a custom PCB carrier for the final radiation test with Linac.

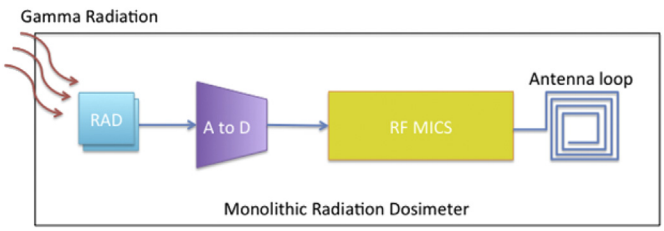

Fig. 1. Block diagram of the monolithic dosimeter.

2.1. CMOS radiation sensors

The radiation-sensing device of this dosimeter consists of an ad hoc modified CMOS Non Volatile Memory (C-FLASH NVM) cell, featuring a floating gate (FG) (Roizin et al., 2008). Additional technical details of the radiation sensor investigated in this project, along with some description of the design of the cells and initial tests results, can be found in Villani et al, (2013).

The use of the FG technology for radiation sensing has been proposed and evaluated earlier, (Tarr et al., 1998; Martin et al., 2001). For this project, a number of different flavors of C-FLASH cells were designed and fabricated, differing in size of the FG and form factor of the MOS transistors, with a view to optimizing their sensitivity to radiation and lower their output noise, Fig. 2. The latest versions of the fabricated cells also implemented, over the FG area, one of the four available metal layers from this CMOS technology, to act as an electrostatic shield and to investigate its effect on sensitivity to radiation when biased to high voltage, Fig. 3. In this technology, the distance between metal layers and FG is approximately 1 μm x metal layer level, with undoped silicon dioxide as separating dielectric. Thus, the application of 10's of volts to any of the layer would generate in the dielectric an electric field of strength of the order of 10^5 V/cm, which increases the escape recombination probability of ions immediately after their generation, (Boch et al., 2006), and, at the same time, does not exceed the breakdown voltage limit for silicon dioxide. The reduced recombination is therefore expected to increase the amount of collected charge by the FG and, thus, to increase the sensitivity. At the same time, the metal layer kept at constant potential acts as an AC ground plane, shunting externally injected noise to ground and, therefore, reducing the output noise of the cell.

Additional cells were also fabricated without FG, to evaluate the sensitivity of this CMOS technology to radiation.

As for all FG based devices, initial charging ('programming' i.e. charge injection in the FG via, for example, a tunneling or channel hot-electron injection process (Lacaze and Lacroix, 2014)) is required to make them sensitive to radiation.

After cell programming, the measurement of the dose of radiation received by the devices is performed, in our case, by measuring the threshold voltage shift of the PMOS transistors at the output inverter of the cell, Fig. 4. The threshold voltage is here conventionally defined as the V_{sd} measured across the transistor when its I_{sd} is set to 1 μA.

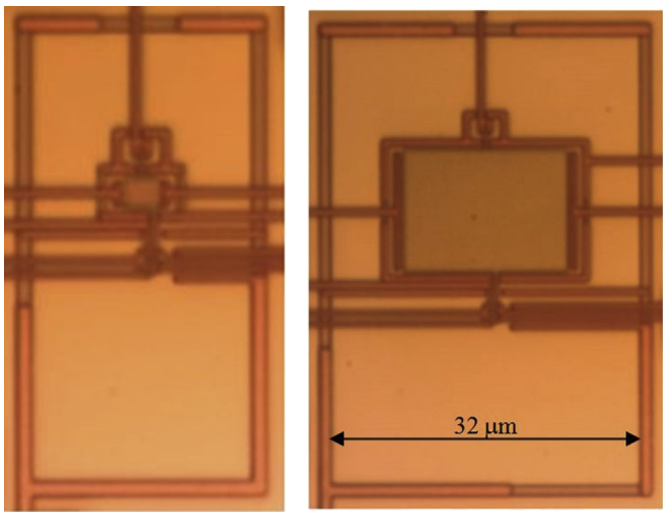

Fig. 2. Microphotographs of two fabricated C-FLASH radiation sensors, with different FG size, to investigate its effects on sensitivity to radiation.

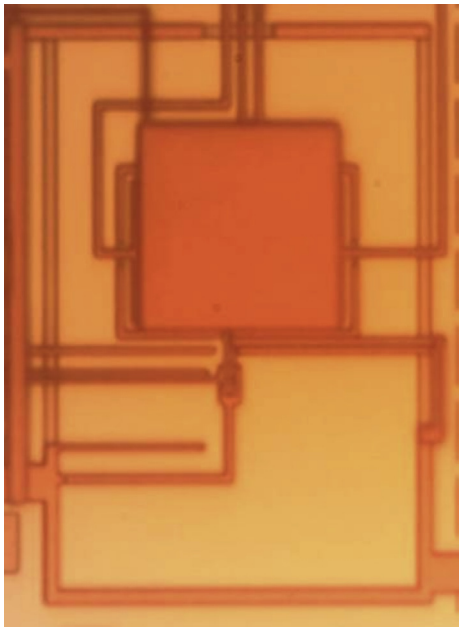

Fig. 3. Microphotographs of a radiation sensor with metal 3 shield ('M3' sensor) over the FG. The shield is accessible via external pads to allow high voltage bias to be applied to it.

2.2. Readout and RF section

The readout section of the dosimeter is built upon a Voltage Controlled Oscillator (VCO), which performs the analog to frequency conversion of the signal from the radiation sensor and an RF section, which includes a ring oscillator operating in the MICS band (FCC Rules and Regulations, 2003). The output of the RF oscillator drives, through a buffer, an integrated loop antenna. A simple voltage reference for the VCO was also implemented in the final design, shown in Fig. 5.

As shown in the schematic, the high impedance output from the radiation sensor is buffered via MOS Q, which also acts as a voltage level translator. The output of the buffer feeds the input of the VCO, the output frequency of which changes as a function of its input voltage in the range of 300 kHz–150 kHz, Fig. 6. The frequency output of the VCO is then applied to a monostable element of fixed output duration, of approximately 200 ns. The output of the monostable enables the RF oscillator for the duration of the pulse width only, to reduce the average power consumption of the circuit. In turn, the output of the RF oscillator is buffered and drives the antenna loop.

Thus, the wireless read out of the dosimeter is performed by measuring, using a remote receiver, the frequency of the MICS bursts, frequency which is directly related to the amount of dose of radiation deposited in the radiation sensor.

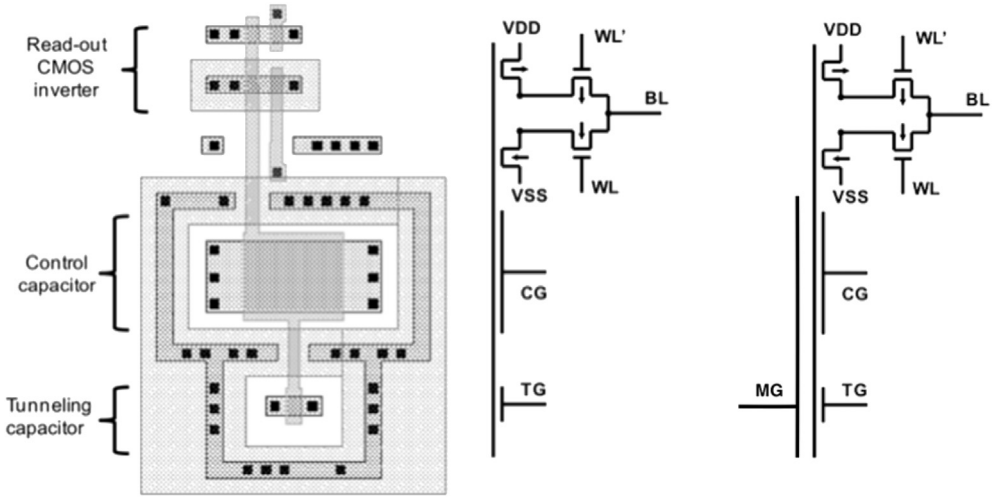

Fig. 4. An example layout of the C-FLASH NVM cell (left), and their electrical diagram (middle and right, with additional metal layer over the FG). The cell structure used in this project includes an output CMOS inverter. The PMOS transistor, biased with 1 μA current, is used for the read out of the cell.

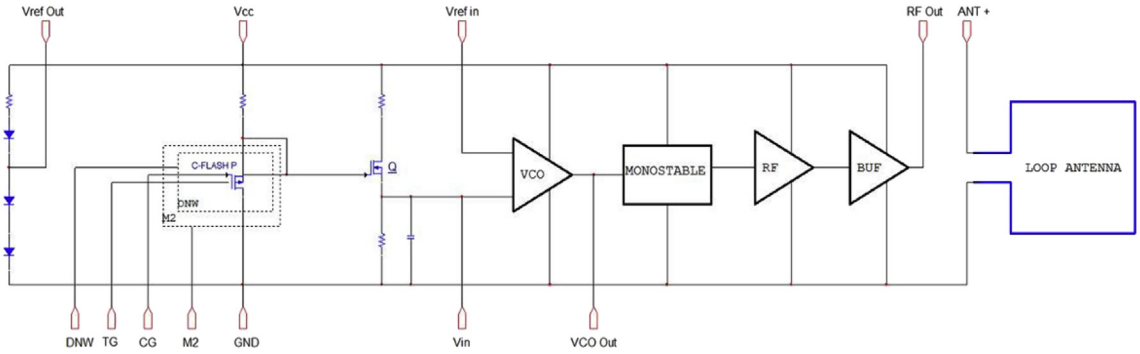

Fig. 5. Schematic diagram of the final circuit of the dosimeter. Some design flavors have the RF out internally connected to the loop antenna and the $V_{ref\ out}$ connected to the $V_{ref\ in}$ of the VCO, to implement a stand-alone system, requiring only the external powering to operate.

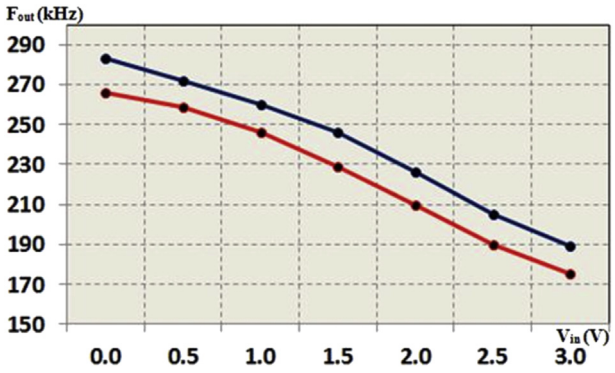

Fig. 6. Cadence simulations of the output of the VCO, pre (red) and post (blue) layout parasitic extraction. (For interpretation of the references to color in this figure legend, the reader is referred to the web version of this article.)

3. Test results of individual blocks

Before testing under a radiation beam, basic electrical tests were performed on the sensors, to evaluate, besides their basic functionalities, their long-term drift after programming and their noise.

Similar tests were performed on the readout blocks, to evaluate the proper functioning of the VCO and the RF oscillator.

3.1. Radiation sensors – electrical test results

A custom DAQ system, based upon a National Instrument PXI 6229 card and Labview control software, was designed and built to perform the full evaluation of the radiation sensors. The DAQ allows the simultaneous setting of the threshold voltages of up to 12 radiation sensor devices in a few seconds with an accuracy of ±2 mV and the real-time recording of their output, Fig. 7.

The usable output voltage range of the designed sensors exceeds 2 V, using a maximum voltage supply of 3.3 V allowed by this technology. Hence, a 1.300 V as the initial voltage threshold for the sensors was chosen.

Once programmed to the initial voltage, the total drift of the threshold voltage of the sensors featuring the additional metal shield over the FG was found not to exceed 5 mV over a period of more than two weeks, Fig. 8. Similar long term drift results, albeit with a slightly higher level of noise, were obtained with the standard cells, not featuring the additional metal shield.

The total noise measured at the output of the standard cells was found not to exceed 80 μV_{rms}, value that includes the input referred noise of the DAQ. The additional metal shield over the FG decreases this value further, reducing it to around 38 μV_{rms}.

3.2. Radiation sensors – radiation test results

Several iterations of radiation tests were performed on individual sensors at the Churchill Hospital, Oxford, UK. Moreover, to improve the statistics, additional tests on batches of more than 2000 devices were performed at the Soroka University Medical Center, Israel.

The test performed on individual sensors consisted of simultaneously irradiating up to 12 devices using a 6 MV photons beam and up to total doses of 225 Gy. Their threshold voltage shifts was monitored during the irradiation phase when biased with a constant current of 1 μA. Further details on the test setup used for these beam tests can be found in Villani et al, (2013). Both type of radiation sensors, with and without the additional metal shield over the FG, were irradiated and tested using the same setup.

Some of the tests results for the sensors with no metal shield are shown in Fig. 9. The left plot shows the average change in output voltage of the sensors as a function of time (effectively dose of radiation, as a constant 5 Gy/minute dose rate was employed for these tests). Interleaved with the irradiation phases, a recovery phase of no irradiation lasting some minutes was introduced, to evaluate the fading in output voltage. The small discrepancy in output voltage among the devices, approximately 23 mV max, is believed to be mostly due to the extra scattering of Compton electrons on the DAQ board, due to the presence of metal tracks, plastic and air gaps. An additional, albeit small, contribution might come from the non-homogeneity of the 6 MV photon beam of field 10×10 cm^2 used, which was measured in a uniform water phantom at 10 cm depth and found to be within 0.7% of the value at the central axis. The right plot shows the extrapolated average sensitivity to radiation of these sensors. An initial sensitivity of approximately 0.6 mV/cGy with a total maximum sigma, among 12 devices, of less than 3% of the measured value was obtained. Despite the usual decrease in sensitivity with accumulated dose, resulting from the discharge of the FG, a resolution in dose of radiation of around 1 cGy is achieved up to doses of 50 Gy.

After delivering a total dose of 50 Gy, the sensors were reprogrammed to the same initial voltage (1.300 V) and the entire irradiation test was repeated. A slight decrease in sensitivity, of

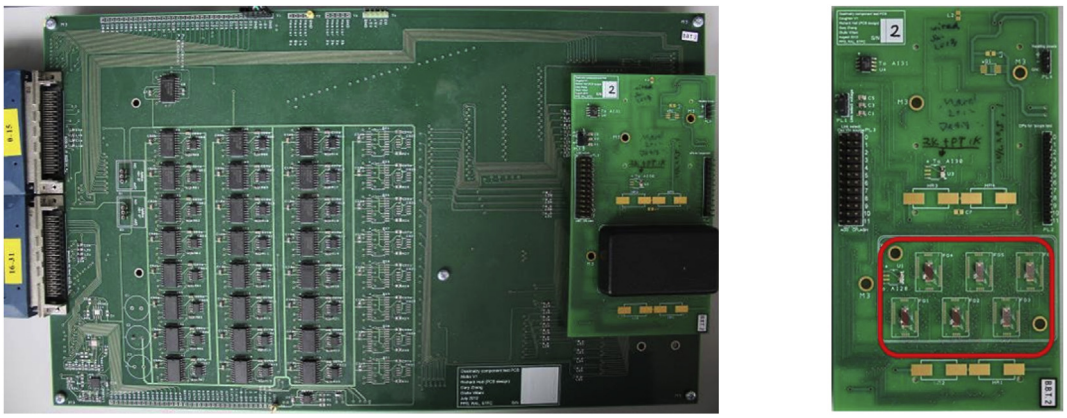

Fig. 7. Pictures of the DAQ Motherboard (left) and Daughter board (right). The Motherboard interfaces with a NI PXI 6229 card and includes analog switches, voltage and current sources for the biasing of the sensors. The Daughter board, which is plugged onto the Motherboard, is populated with up to six individual ASICs (enclosed in the red rectangle in the picture) and includes also three temperature sensors, to evaluate temperature effects on the sensors. (For interpretation of the references to color in this figure legend, the reader is referred to the web version of this article.)

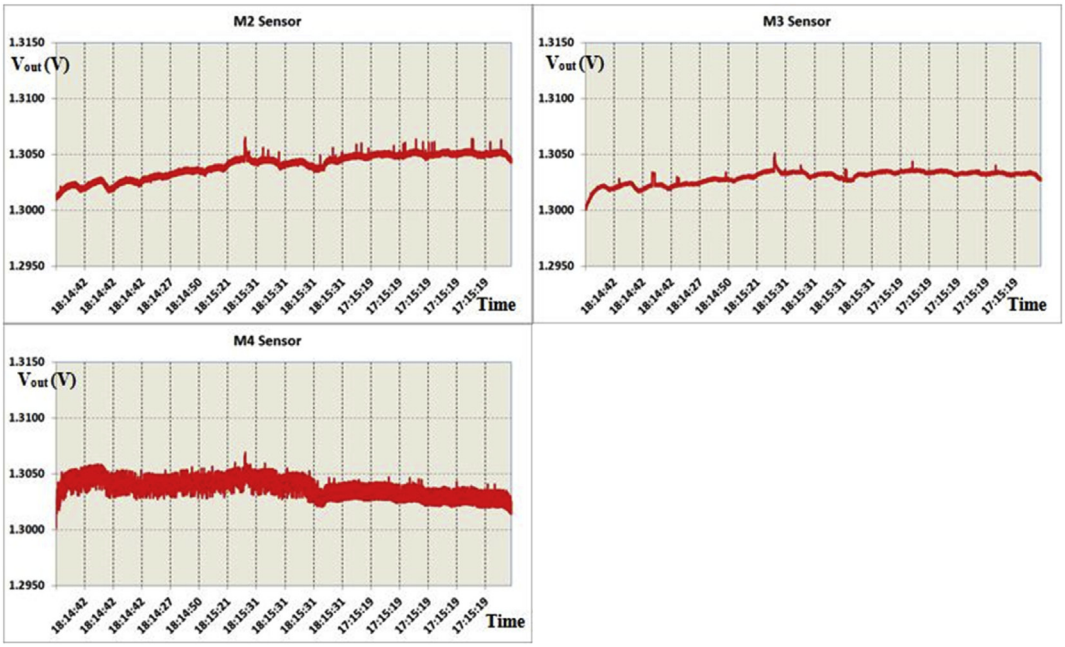

Fig. 8. Example plots of the voltage output stability of the radiation sensors over a period of around 15 days. The sensors were programmed to 1.300 V and kept biased with I_{sd} current of 1 μA. The metal layer shields were biased to 60 V (M4), 30 V (M3) and 20 V (M2) respectively. A small daily variation in the sensor's output due to temperature fluctuations can be seen.

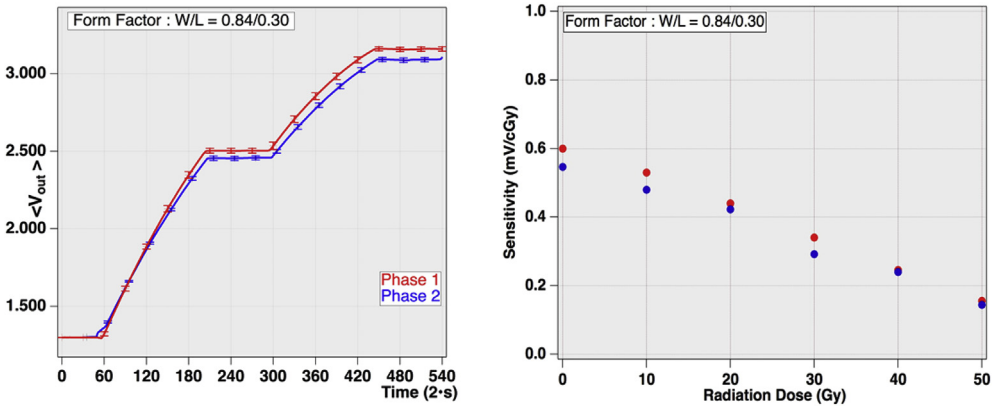

Fig. 9. The left plot shows the averaged output and σ deviation (error bars) of the sensors vs. time during the first (red) and, following re-programming, second (blue) irradiation phase, with each phase delivering a total dose of 50 Gy. The rest phase in between irradiation (flat curves) shows no measurable sign of output fading. The right plot shows the extrapolated average sensitivity vs. accumulated dose for the first (red) and second (blue) irradiation phase. (For interpretation of the references to color in this figure legend, the reader is referred to the web version of this article.)

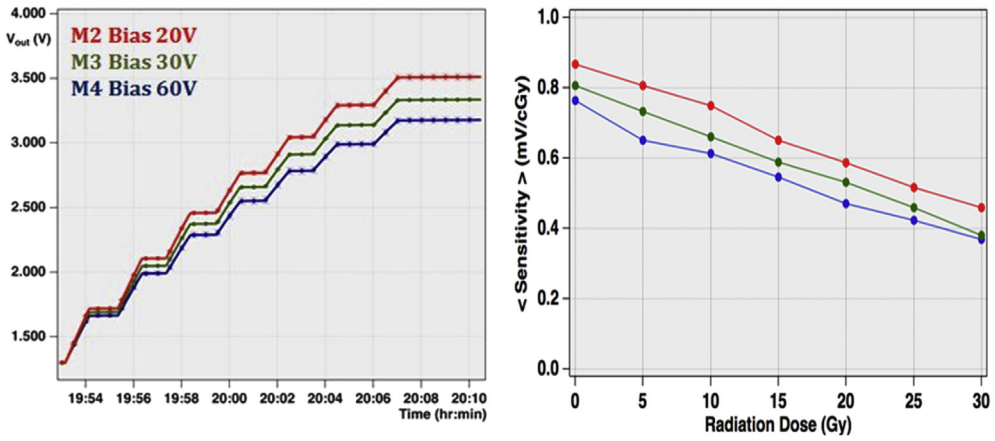

Fig. 10. The average threshold voltage shift (left) and sensitivity variation (right) of the sensors with additional metal shields over the FG biased at different voltages. On the left picture, each threshold change increment corresponds to a dose of 5 Gy delivered over 1 min, followed by 1 min fading study. The total dose delivered was 35 Gy.

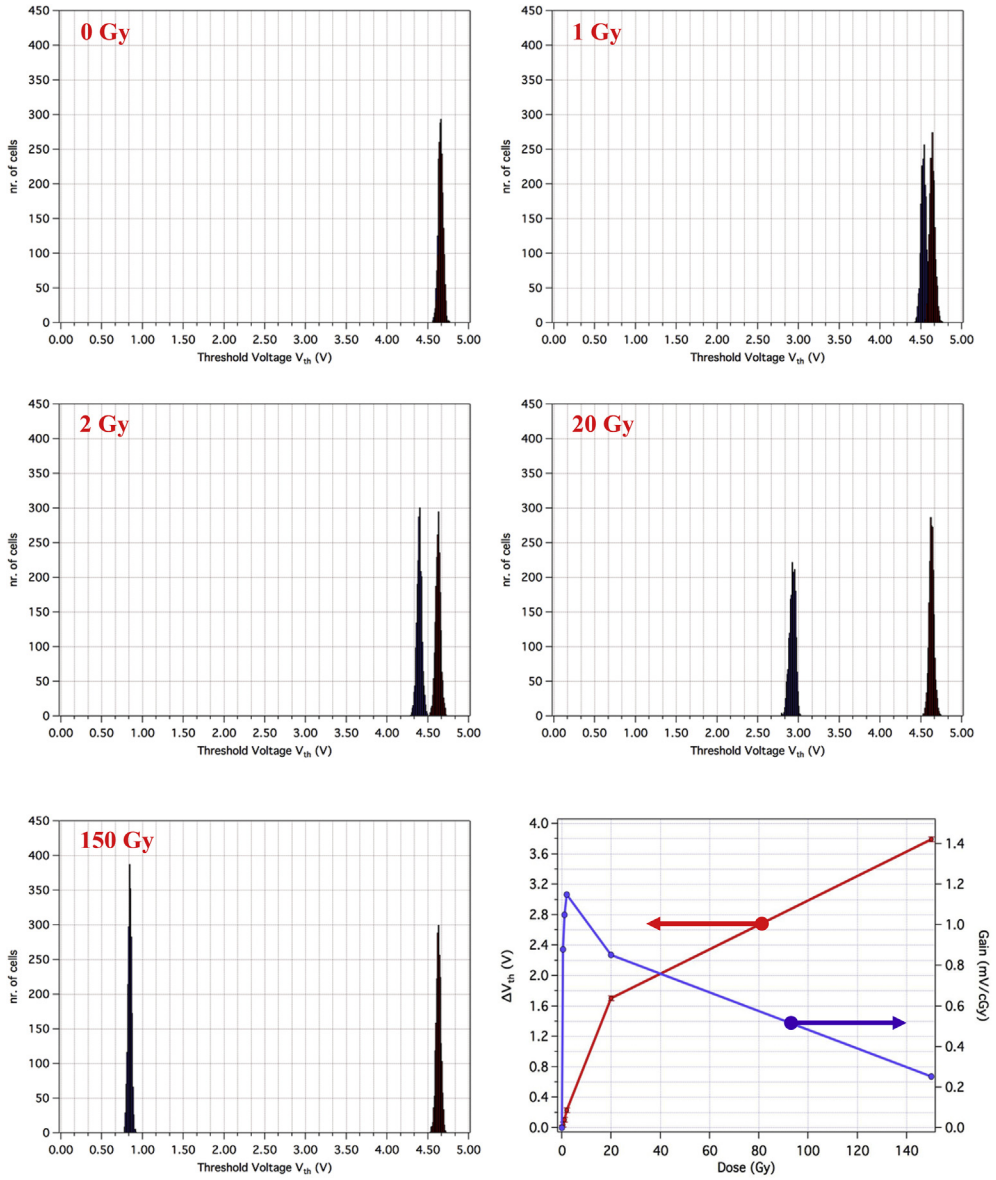

Fig. 11. Histogram plots of the threshold voltage of sensor arrays before and after irradiation for different gamma doses, with each array consisting of >2000 devices. Bottom right plot shows the dose response (red curve) and extrapolated sensitivity (blue curve) of the arrays. After programming, the arrays of devices were irradiated using a ^{60}Co source up to doses of 150 Gy. The un-irradiated batch of sensors shows threshold voltage drift comparable to that found by testing individual devices over a period of two weeks. (For interpretation of the references to color in this figure legend, the reader is referred to the web version of this article.)

approximately 5% maximum for all the flavors of sensors investigated, is observed in the subsequent cycle of irradiation. This effect is believed to be due to the generation and subsequent filling of hole-traps at the $Si-SiO_2$ interface of the FG. This layer of positive charge, decreasing the strength of the electric field extending into the dielectric, limits the charge collection by the FG from the region of dielectric above. Nonetheless, owing to the low noise at the output of the sensors, a resolution in dose of radiation of around 1 cGy is still achieved.

The results of the tests on the individual sensors featuring the additional metal shield are shown in Fig. 10. These sensors were programmed to the same initial voltage of 1.300 V used for the sensors with no metal shield. The left plots shows the average output of the various sensors vs. dose of radiation and the right plots shows the extrapolated sensitivity. For this test the metal shields were biased at different voltages: the sensors with metal 4 shield ('M4') were biased to 60 V, those with metal 3 shield ('M3') used 30 V and 20 V was used for those with metal 2 shield ('M2'). The bias voltage applied to the metal shield affects the potential of the FG via capacitive coupling, which requires further injection of electrons into the FG to achieve the same initial value of threshold voltage. Care was taken to ensure that these bias voltages were not high enough to ignite tunneling of charge from the FG into the silicon substrate, which could have spoilt the radiation sensitivity tests.

As expected, the test results showed that, despite an inherent decrease in sensitivity due to the increased capacitance of the FG, by proper biasing the metal shield the sensitivity to radiation increases up to approximately 0.87 mV/cGy for the M2 sensor. This higher sensitivity stems from the increased strength of the electric field in the region of thick dielectric above the FG, which helps collecting the charge generated by the incoming radiation by the FG. Conversely, by keeping the metal shield grounded, a reduction in sensitivity is observed.

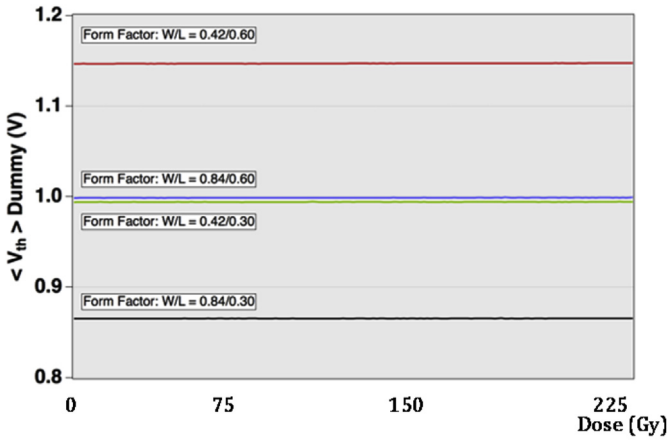

Flavor	V_{th} shift (mV)	Sens (mV/cGy)
W/L= 0.42/0.60	0.8	$0.35 \cdot 10^{-4}$
W/L= 0.84/0.60	2.6	10^{-4}
W/L= 0.42/0.30	5.8	$2.5 \cdot 10^{-4}$
W/L= 0.84/0.30	3	$1.3 \cdot 10^{-4}$

Fig. 12. Average threshold voltage shifts with dose of radiation of devices not featuring FG but with the same output MOS transistors layout and for different MOS form factors. Negligible changes, of the order of ≈1 mV, were observed for doses up to 225 Gy.

The array of more than 2000 devices on wafers were pre-programmed at the semiconductor foundry and delivered to the irradiation center, where they were irradiated using a ^{60}Co source to different level of dose of gamma radiation up to 150 Gy. The histogram plots of Fig. 11 show the shift and the spread of the threshold voltage of the devices irradiated with gamma doses of 1, 2, 20, 150 Gy respectively. The small change of the spread over the entire range of dose confirms the very good uniformity of sensitivity to radiation of these devices, as already found from the individual sensor tests. The top left plot of Fig. 11 shows the histogram plot of threshold voltage of non-irradiated devices, measured after the same interval of 2 weeks taken to complete the irradiation test. The average shift of approximately 5 mV over such period closely matches what measured from the tests of the individual devices and confirms their good long term stability. The higher radiation sensitivity measured from the arrays, bottom right plot of Fig. 11, compared to the results of the individual cells, right plot of Fig. 9, is explained by the different readout method that has been used for the individual sensors of the array. Instead of measuring the threshold voltage shifts of each individual PMOS of the cell, the $V_{th\text{-}50}$, or mid-point output voltage of the inverter, was measured, using both the N and P MOS transistors of the structure.

Additional beam tests were performed on devices not featuring the FG, to evaluate the sensitivity to radiation of this CMOS technology. Negligible changes were observed in the threshold voltage of the devices irradiated up to 225 Gy, as shown in Fig. 12.

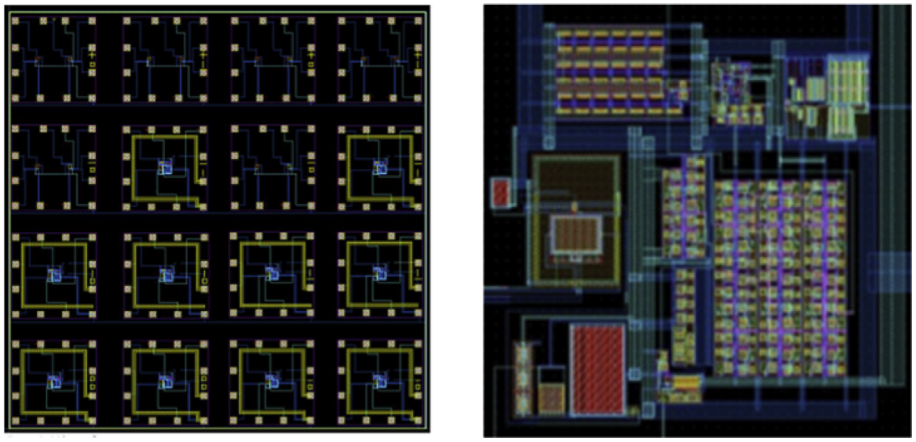

Fig. 13. Layout of the final design of the dosimeter, which included sensor-only flavors and different internal antenna arrangement (left). A magnification of the dosimeter active circuitry is shown on the right picture.

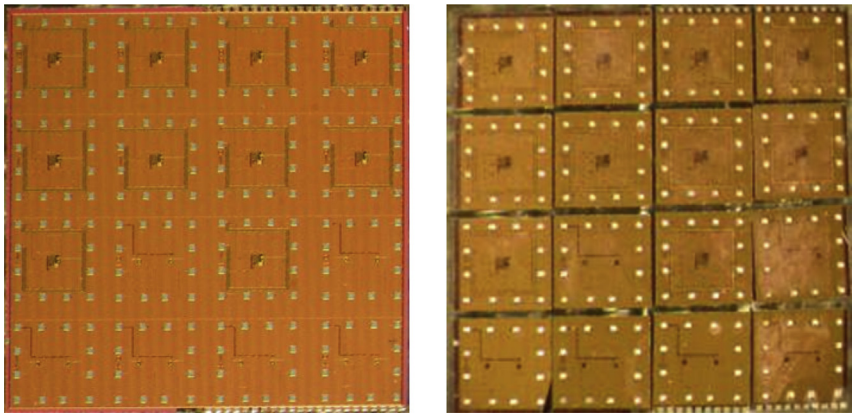

Fig. 14. Picture of a whole 5 × 5 mm^2 ASIC (left) and 1 × 1 mm^2 individual dosimeters, obtained through mechanical dicing (right).

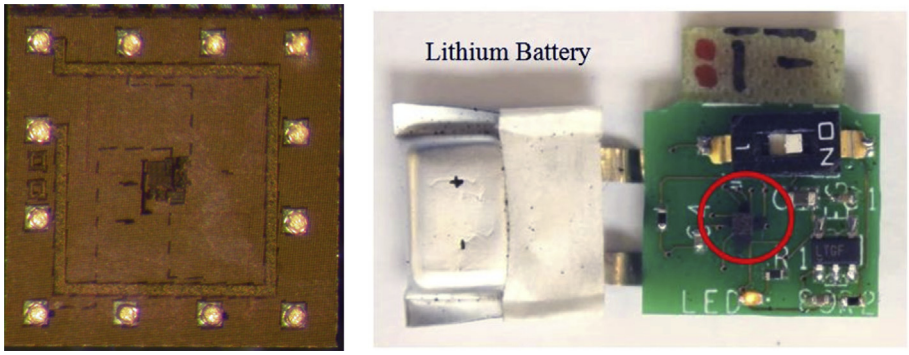

Fig. 15. Magnification of a diced 1× 1 mm^2 dosimeter, with Au studs on the pads (left) and picture of the flipped bump-bonded dosimeter on the carrier PCB for its final testing (right). The 1 × 1 mm^2 dosimeter ASIC is circled in red. (For interpretation of the references to color in this figure legend, the reader is referred to the web version of this article.)

3.3. Readout section – RF test results

Initial tests were performed on ASICs wire bonded on a PCB carrier to evaluate the proper functioning of the RF oscillator, designed to operate in the MICS band. Using an RF setup previously described, (Villani et al., 2014), test results indicated that the RF signal was detectable from around 1 m away from the dosimeter, in the wire bonded configuration. However, as higher efficiency in RF transmission could not be excluded, owing to the presence of the bond wires, more realistic tests were postponed until the bump bonded version of the dosimeter was available.

4. Final implementation of the monolithic dosimeter

The third and final design of the dosimeter includes the sensor and the read out elements, previously designed and tested, in a single circuit. Different antenna flavors and sensors with and without metal shields above the FG were also included in the design of the final ASIC, Fig. 13.

Some of the 5 × 5 mm^2 fabricated ASICs were diced to the required 1 × 1 mm^2 size, Fig. 14 and initially wire bonded on a small PCB carrier for the preliminary electrical test, to evaluate the proper working of all the sections of the dosimeter and the reliability of the dicing process.

After successful evaluation of the wire bonded devices, some ASICs were selected for bump bonding on a PCB carrier for the final radiation test. In preparation for the bonding, single dies of 1 × 1 mm^2 were cleaned with 3 min immersion in acetone, followed by 2 min in ethanol and 3 min in DI water, before a final cleaning with dry nitrogen. Next, Au studs, of approximately 70 μm diameter and 60 μm thickness, were applied to all the twelve pads of each dice and conductive epoxy, of approximately 160 μm diameter and 30 μm thickness, was placed on each bond pad. A flip-chip bonder FC150 was used for the alignment and bonding operation. Once bonded onto the PCB, the devices were cured at 100 °C for 12 h.

A picture of the final device, with the 1 × 1 mm^2 die bump-bonded on the PCB carrier, is shown on Fig. 15.

The small PCB carrier was designed to hold the dosimeter and includes all the remaining components needed for the online test, namely a switch to enable powering of the device, an LED, some passive components of pull-up and a voltage regulator, to stabilize the voltage from the battery. An external rechargeable lithium cell provided powering to the dosimeter during the online tests.

The tests with bump bonded 1 × 1 mm^2 devices also served the purpose of demonstrating the possibility, using this technique, of reducing the total footprint occupied by the dosimeter, which could, for example, include attachable power source to the ASIC itself.

Functionality tests on the bump bonded devices, which included programming of the radiation sensor and evaluation of their stability and drift, showed that, out of eight devices initially bonded, seven worked as expected and one had issues with the RF oscillator not related to the bonding.

5. Wireless test of the monolithic radiation dosimeter

As described above, the implemented method of wireless read out of the dosimeter is based on measuring the frequency of the transmitted MICS bursts.

As the MICS frequency corresponds to a wavelength of approximately 75 cm, much bigger than the overall size of the dosimeter and, therefore, of the integrated antenna, the efficiency in RF transmission is very low. In order to receive the weak RF signal emitted by the monolithic dosimeter, a sensitive external RF receiver had to be used.

The RF receiver setup for the online tests consisted of an ETS-Lindgren 7405-901 loop probe connected to a Femto DUPVA-1-60 RF amplifier and an Agilent E4411B spectrum analyzer. The analyzer was connected, via GPIB port, to a PC, on which ran a Labview program for the analysis of the received data.

Preliminary tests performed in our lab showed that, with the described equipment, the carrier RF signal was detectable from the bump-bonded dosimeter device at a distance of approximately

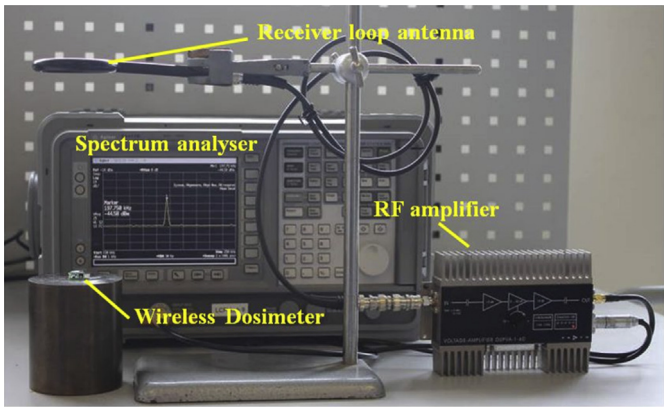

Fig. 16. The external receiver for the online tests consists of a 6 cm loop antenna, connected to an RF amplifier and a spectrum analyzer. In free air an RF signal of approximately −90 dB$_m$ amplitude from the bump-bonded dosimeter is detected at a distance of ~10 cm. A Labview program on a remote PC retrieves the data from the spectrum analyzer for further processing, plotting and saving.

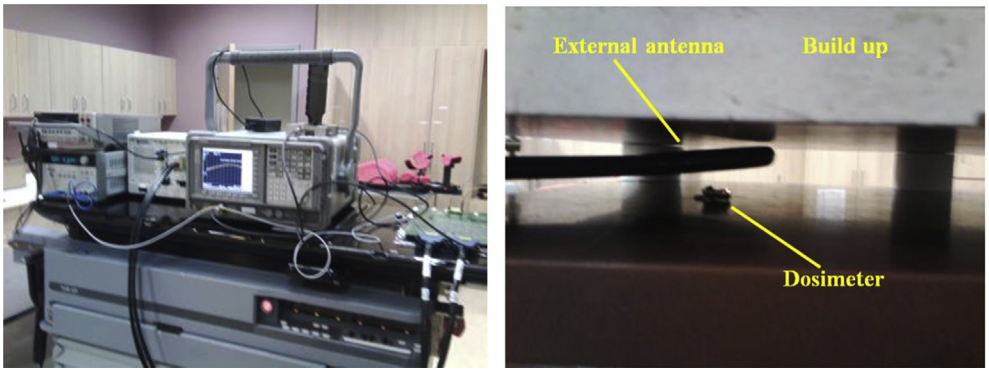

Fig. 17. For the online test each dosimeter was placed in between the water equivalent material, in close proximity to the antenna receiver (right) and irradiated using a 6 MV photon beam. The dose of radiation measured was retrieved from the dosimeter using the RF receiver setup (left).

10 cm in free air, Fig. 16. As reported on a previous paper (Villani et al., 2013), RF tests were also performed to evaluate potential sources of noises in the MICS band caused by Linac machines when operating, which could have spoilt the detection of the weak RF signal emitted by the dosimeter.

The final radiation test, with real-time readout each 5 s, was carried out on two dosimeters using a 6 MV Linac at the Churchill Hospital, Oxford, UK. Using a similar setup as per previous sensors tests, each dosimeter was placed between 5 cm thick slabs of the water equivalent material Gammex RMI457. The photon beam size was set to a 4×2 cm^2 multileaf collimator (MLC) field with a 4×3 cm^2 of jaws backup. The photon energy used for all tests was 6 MV, and the dose rate set to 500 monitor unit (MU). The external receiver loop antenna had to be placed in between the slabs of water equivalent layers, close to dosimeter, at approximately 2–3 cm from the device, Fig. 17.

The dosimeter readout rate was dictated by the limited bandwidth in data retrieval from the spectrum analyzer. During the online radiation test the Labview program retrieves the burst of data from the spectrum analyzer and implements a Gaussian fitting to identify the frequency at which the peak amplitude of the RF signal occurs. As described before, the change in frequency of the measured peak signal is directly related to the amount of dose of radiation deposited in the dosimeter. Owing to the electrical noise, up to ten data samples are averaged before performing the Gaussian fitting, to improve the frequency resolution with which the peak amplitude of the RF signal can be measured.

Output signal vs. time, as measured during the wireless test of the two dosimeters tested, are shown on Fig. 18. Both dosimeters were irradiated up to 30 Gy, using the same temporal pattern of 1 min of irradiation followed by 1 min of rest, to evaluate fading of the output signal, as done during the tests of the radiation sensors only. In all cases, no detectable occurrence of fading was observed.

6. Summary and conclusions

A monolithic wireless radiation dosimeter has been proposed, designed and fabricated in a standard 180 nm CMOS technology and tested in a real clinical environment.

Owing to its size, of 1 mm^3 only, the device could potentially find applications in the field of Linac radiotherapy, as an implantable dosimeter. The implemented method of read out of the dosimeter is wireless, using RF transmission in the MICS band.

Radiation tests results, performed with medical Linac in a clinical environment on preliminary versions of dosimeter, confirmed the suitability of the proposed technology for the fabrication of the radiation sensors and the read out electronics implemented in this

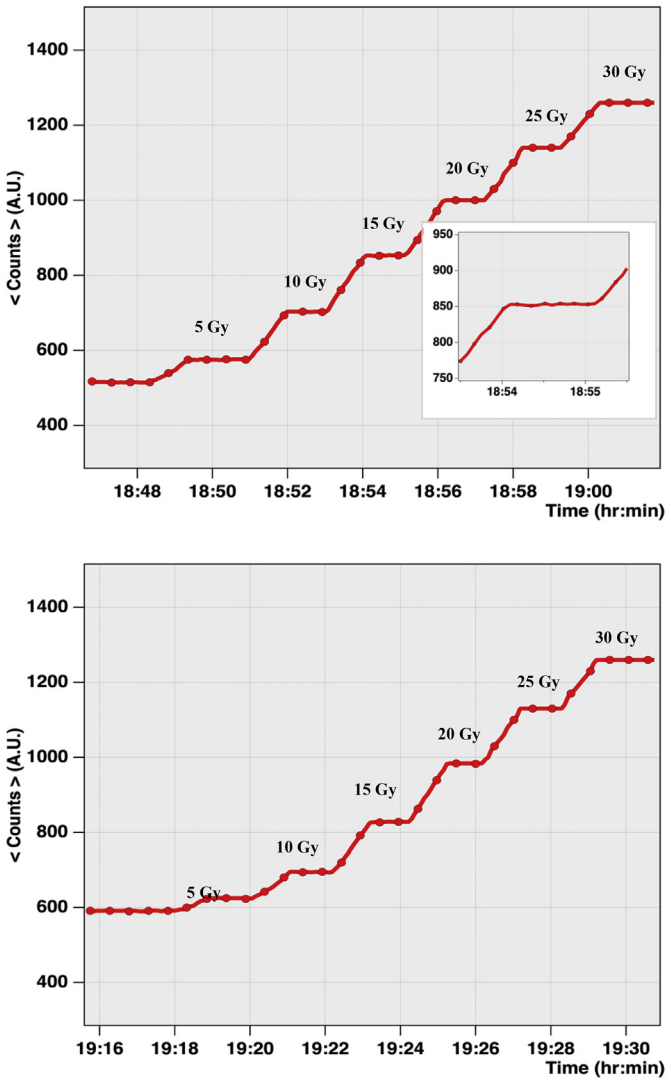

Fig. 18. Real-time average outputs from the two M2 type dosimeters as measured wirelessly during the radiation test. The Y axis shows the frequency change of the peak signal as detected by the receiver, with each point representing 50 Hz drift (the ~100 kHz output range of the VCO was divided into 2000 points for this test). The M2 FG shield was connected to ground on the PCB carrier, therefore reducing the overall sensitivity to radiation. The minimum dose increment achieved during this test was ~3 cGy. The inset in the top picture shows a magnification of the output after 15 Gy of delivered dose to the first dosimeter, showing no detectable evidence of fading.

1 mm^3 size dosimeter. A dose resolution better than 1 cGy with accuracy better than 3% over a 50 Gy dose range was demonstrated in case of direct galvanic readout of the dosimeter. Immediately after irradiation no sign of fading of the output from the radiation sensors was observed. Additional tests performed on arrays of >2000 devices confirmed the sensitivity and good reproducibility of the radiation sensors characteristics. Additional long term tests on the sensors evaluated their threshold voltage drift to around 5 mV over a period of more than two weeks. The obtained results allow prescription of a unique sensitivity to a whole batch of dosimeters, essentially simplifying the calibration procedure.

Several of the final incarnations of the dosimeter were mechanically diced to 1×1 mm^2 and bump-bonded on a PCB carrier for the wireless radiation tests.

The final tests were performed in a hospital using a 6 MV photon beam and successfully demonstrated the possibility of wireless real-time readout of the dose of radiation delivered to the devices.

Future issues to address, to render such proposed solution a viable QA and plan verification tool in radiotherapy applications, would include the autonomous powering, the study of biocompatible packaging of the dosimeter, response with depth once immersed in water and its effect on radiation sensitivity and RF transmission.

Despite the remaining, and no doubt challenging, technical issues, it is believed that such an approach is feasible and could indeed prove to be very useful as QA tool in radiotherapy applications.

Acknowledgments

This work was funded by a STFC UK CLASP funding (Grant reference ST/I003290/1). Particular thanks are due to Andy Buckle at Churchill Hospital, Oxford, UK, for his technical help and valuable support.

References

Boch, J., Saigne, F., Dusseau, L., Schrimpf, R.D., 2006. Temperature effect on geminate recombination. Appl. Phys. Lett. 89, 042108.
FCC Rules and Regulations, Jan. 2003. MICS Band Plan", Part 95.
https://www.rcr.ac.uk/towards-safer-radiotherapy.
International Atomic Energy Agency, 2000. Absorbed Dose Determination in External Beam Radiotherapy, Technical Reports Series No. 398. IAEA, Vienna (.
International Atomic Energy Agency, 2007. Absorbed Dose Determination in External Beam Radiotherapy: an International Code of Practice for Dosimetry Based on Standards of Absorbed Dose to Water, Technical Reports Series No. 457. IAEA, Vienna (.
Izewska, J., Svensson, H., Ibbot, G., 2002. Worldwide quality assurance networks for radiotherapy dosimetry. In: Proc. Int. Symp. Standards and Codes of Practice in Med. Rad. Dosim., IAEA-CN-96/76. IAEA, Vienna, pp. 139–156.
Lacaze, P.C., Lacroix, J.C., 2014. Non Volatile Memories. John Wiley & Sons. ISBN: 184216238.
Mahadevappa, M., 2009. MDCT Physics: the Basics – Technology, Image Quality and Radiation Dose. ISBN: 9780781768115.
Martin, M.N., Roth, D.R., Garrison-Darrin, A., McNulty, P.J., Andreou, A.G., Dec. 2001. FGMOS dosimetry: design and implementation. IEEE Trans. Nucl. Sci. 48 (12), 2050–2055.
Nelms, B., Simon, J., 2007. A survey on planar IMRT QA analysis. J. Appl. Clin. Med. Phys. 8 (3).
Roizin, Y., Aloni, E., Birman, A., Dayan, V., Fenigstein, A., Nahmad, D., Pikhay, E., Zfira, D., May 2008. C-Flash: an ultra-low power single poly logic NVM", non-volatile semiconductor memory workshop. In: 2008 and 2008 International Conference on Memory Technology and Design. NVSMW/ICMTD 2008. Joint, 18-22, pp. 90–92.
Rosenfeld, A.B., et al., 2006. Radiat. Protec. Dosim. 120 (1–4), 48–55.
Scarantino, C.W., et al., 2004. An implantable radiation dosimeter for use in external beam radiation therapy. Med. Phys. 31, 2658–2671.
Scarantino, C.W., et al., 2005. Initial clinical results of an in vivo dosimeter during external beam radiation therapy. Int. J. Radiat. Oncol. Biol. Phys. 62 (2), 606–613.
Scarantino, J., et al., 2006. True in-vivo dosimetry. Inter. Journal of Rad. Onc. Biol. Phys. 66 (Issue 3).
Scarantino, C.W., et al., 2008. The observed variance between predicted and measured radiation dose in breast and prostate patients utilizing an in vivo dosimeter. Inter. J. Rad. Onc. Biol. Phys 72 (2), 597–604.
Shamim, A., Arsalan, M., Roy, L., Shams, M., Tarr, G., July 2008. Wireless dosimeter: system-on-chip versus system-in-package for biomedical and space applications. IEEE Trans. CAS-II Express Briefs 55 (7).
Tarr, N.G., Mackay, G.F., Shortt, K., Thomson, I., Jun. 1998. A floating-gate MOS dosimeter requiring no external bias supply. IEEE Trans. Nucl. Sci. 45 (6), 1470–1474.
Villani, E.G., Crepaldi, M., DeMarchi, D., Gabrielli, A., Khan, A., Pikhay, E., Roizin, Y., Rosenfeld, A., Zhang, Z., 2013. Monolithic 180 nm CMOS dosimeter for in vivo medical applications. IEEE Trans. Nucl. Sci. 60 (Issue. 2), 843–849.
Villani, E.G., Crepaldi, M., DeMarchi, D., Gabrielli, A., Khan, A., Pikhay, E., Roizin, Y., Rosenfeld, A., Zhang, Z., Dec. 2014. A monolithic 180 nm CMOS dosimeter for in vivo dosimetry medical applications. Rad. Meas. 71 (Issue. 2), 389–391.